Results from One Year of Ka-band Beacon Measurements at Svalbard

James Nessel, NASA Glenn Research Center, Cleveland, OH 44135,
+1 216-433-2546, james.a.nessel@nasa.gov

Xavier Boulanger, ONERA French Aerospace Laboratory, Toulouse, France,
+33 5-6225-2880, xavier.boulanger@onera.fr

Laurent Castanet, ONERA French Aerospace Laboratory, Toulouse, France,
+33 5-6225-2729, laurent.castanet@onera.fr

Torgeir Prytz, Kongsberg Satellite Services, Longyearbyen, Norway,
+47 79025588, torgeir@ksat.no

Antonio Martellucci, European Space Agency, Noordwijk, Netherlands,
+31 71-565-5603, antonio.martellucci@esa.int

Abstract

Since April 1, 2016, a Ka-band (20.198 GHz) propagation terminal has been installed and operating at the Svalsat facility in Longyearbyen, Norway. This campaign is a joint effort between the European Space Agency (ESA), Kongsberg Satellite Services (KSAT), the French Aerospace Laboratory (ONERA), the Centre National d'Etudes Spatiales (CNES), and NASA Glenn Research Center (GRC) to characterize atmospheric attenuation, scintillation, and depolarization in the Ka-band in high latitude regions at low elevation angles. The propagation terminal observes the Thor 7 20.198 GHz RHCP beacon at nominally 2.6 deg elevation angle. Simultaneous 10 Hz and 1 Hz sampling is performed and a total dynamic range of 35 dB is achieved. One year of propagation data has been collected and the preliminary results are presented in this paper. From the first year of measurements, it is observed that at these low elevation angles, strong scintillation/multi-path conditions, as well as significant depolarization events can occur which may impose difficulties in meeting mission link acquisition requirements at 5 deg elevation angle, such as those desired by the Joint Polar Satellite System (JPSS) mission. The design of the dual-polarized terminal with integrated digital radiometer, as well as the data processing techniques are described, along with the first year results and preliminary conclusions.

Introduction

The amount of data being collected and requiring download for Earth Observation (EO) missions are dramatically increasing year by year. Historically, EO satellites make use of the X-band for their downlink frequency. However the limited bandwidth available and the increasing congestion of this band is becoming problematic for these missions that require an ever-increasing amount of data to deliver. This situation is now pushing next generation EO missions to utilize the Ka-band (25.5-27 GHz) to support their needs. Furthermore, to fully support data volume requirements, some of these missions are being driven to dual polarization and lower elevation angle acquisition (down to 5 deg).

Presently, the Joint Polar Satellite System (JPSS), of which JPSS-1 has already launched in November 2017, is the first to operationally use Ka-band for direct-to-Earth downlinks at high latitude ground station sites. Following JPSS-1, a number of additional missions will also begin the transition to Ka-band direct-to-Earth data downlinks as their primary spectrum. These missions include, but are not limited to, the Meteorological Operational Satellite – Second Generation (MetOp-SG) satellite, the NASA/ISRO Synthetic Aperture Radar (NISAR) satellite, the Plankton, Aerosol, Cloud, ocean Ecosystem (PACE) satellite, and others slated to launch in the 2019-2022 timeframe. This burgeoning growth in Ka-band utilization at high latitude ground stations necessitates atmospheric characterization of the polar climate in order to effectively design communications systems for high reliability data downlinks at low elevation angles.

Since April 1, 2016, a Ka-band (20.198 GHz) propagation terminal has been installed and operating at the Svalsat facility in Longyearbyen, Norway. This campaign is a joint effort between the European Space Agency (ESA), Kongsberg Satellite Services (KSAT), the French Aerospace Laboratory (ONERA), the Centre National d'Etudes Spatiales (CNES), and NASA Glenn Research Center (GRC) to characterize atmospheric attenuation, scintillation, and depolarization in the Ka-band in high latitude regions at low elevation angles. This data will then be used to validate and/or develop new models for high latitude regions and support the communications system design for the next generation of EO missions utilizing Ka-band. In this paper, we describe the experimental setup and beacon receiver hardware. Calibration routines implemented to derive statistical products are discussed and the first year results and preliminary conclusions are presented.

Site Description: Longyearbyen, Svalbard

The NASA beacon receiver is installed at the site designated SG61, located at the east end of the Svalsat complex, as shown in the photograph of Figure 1. The Svalsat facility sits atop a plateau approximately 500 m above the sea level at 78.2 deg N latitude. This facility represents one of the few polar orbiting ground station support sites and due to its high latitude location, typically possesses the longest access times available for polar orbiting missions.

Prior to installation of the beacon receiver hardware at SG61, a multichannel PR-2330 Polarimetric Radiometer, developed by Radiometrics, and a NASA weather station had been in operation there since May 2011. The radiometer measurements provided good statistics for gaseous and cloud attenuation for several years [1]. The addition of the beacon receiver in 2016 has now allowed for the characterization of hydrometeor attenuation, scintillation, and depolarization in conjunction with the radiometric measurements.

Figure 1. Aerial photograph of the Svalbard NEN site showing the location of SG61.

The beacon receiver is housed inside a radome atop a 3-m post, as shown in the photograph of Figure 2. Several satellites were investigated as potential candidates for propagation measurements from the site, but horizon mask limitations from the site (see Figure 3), resulted in the choice of Thor-7. Thor-7 transmits a continuous wave RHCP beacon at 20.198 GHz and resides at a fixed elevation angle from the site of nominally 2.6 deg. Its location places it right in a local valley between two mountain tops.

Additionally, the existing weather station at the site was updated to include a Lambrecht 1518 H3 rain gauge and an ORG-815 optical rain gauge for the measurement of rain rate at the site.

Figure 2. Photograph of 1.2-m antenna mounted inside radome at SG61.

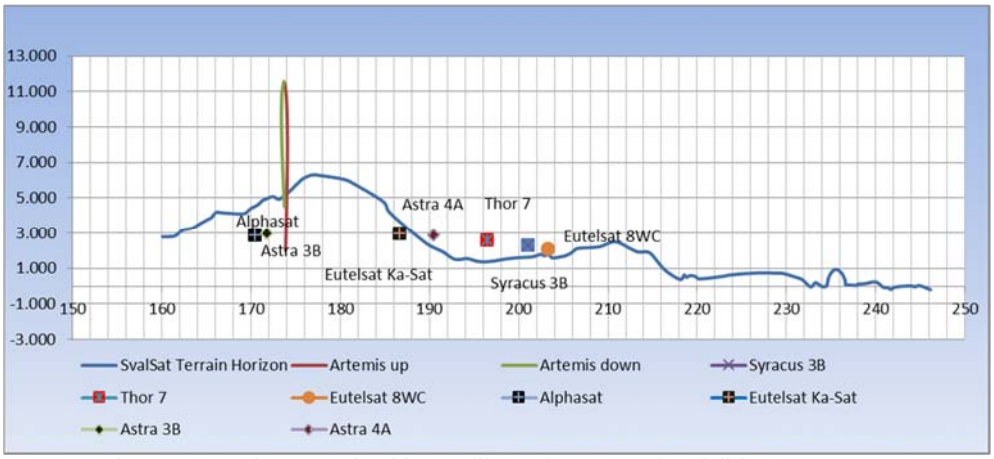

Figure 3. Horizon mask with satellites of opportunity visible from SG61.

Beacon Receiver System Design

The system block diagram for the NASA beacon receiver is shown in Figure 4. A 1.2-m Cassegrain reflector antenna with an adjustable polarizer splits the receive signal via an orthomode transducer (OMT) for the collection of both the co-polar (RHCP) and cross-polar (LHCP) 20.198 GHz beacon signal. A low noise amplifier (LNA) with nominal gain of 44 dB and 1.4 dB noise figure is used and the resulting co/cross-pol signals are downconverted to an intermediate frequency (IF) of 69 MHz. The 69 MHz signals are sent via RF over fiber to a centralized facility where the signals are digitally bandpass sampled at 3.1 MSPS. A frequency estimation routine described in [2-3] is implemented resulting in a measurement bandwidth of 11.7 Hz which is recorded at a rate of 10 Hz and 1 Hz. Furthermore, as described in [3], a noise power measurement technique is implemented to provide a backup and demonstrate the utility of noise power integration for radiometric measurements. This technique provides a relatively small bandwidth of 1 MHz and approximately 1 sec integration time, resulting in a sky brightness temperature resolution of approximately 1 K.

The effective isotropic radiated power (EIRP) of the Thor-7 beacon was specified to be nominally 19 dBW at edge of coverage, which was confirmed during system checkout. The resulting dynamic range performance of the system was experimentally verified to be approximately 35 dB.

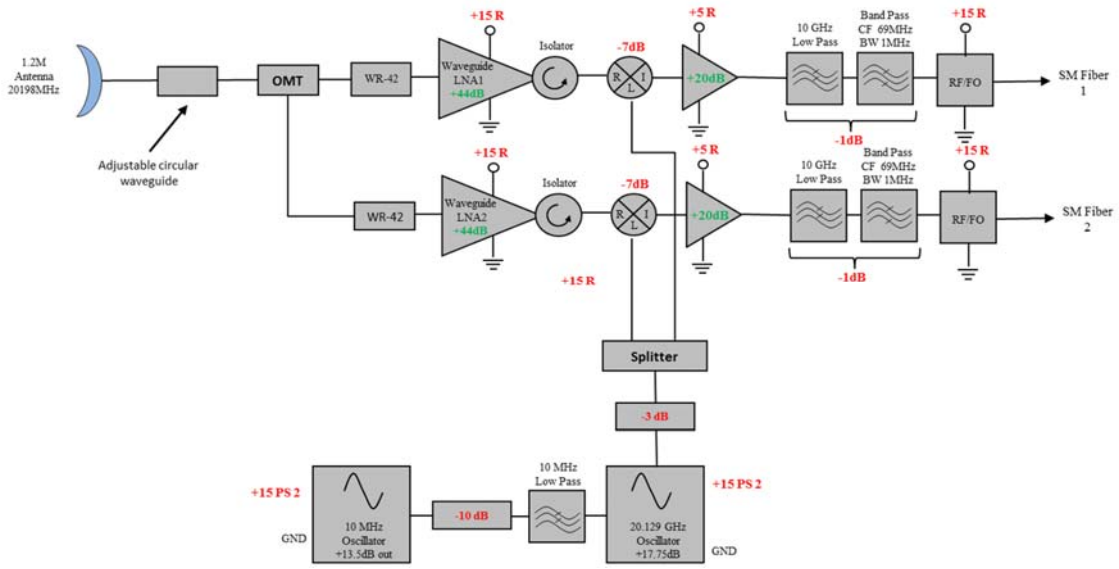

Figure 4. System block diagram of the NASA beacon receiver.

Clear Sky Calibration Procedure

The calibration of the measured attenuation level to derive total atmospheric attenuation is performed following the procedure described in [4]. In summary, the FFT of the 1 MHz bandpass sampled signal is integrated over the noise spectrum, following a notch filter to remove the beacon signal, and recorded at a 1 sec integration time. The integrated noise power time series effectively functions as a low resolution microwave radiometer directly at the operation frequency of 20.198 GHz. Conversion of the integrated noise power measurement to a sky brightness temperature (and eventually an atmospheric attenuation) involves coarse calibration of the beacon signal using the European Centre for Medium Range Weather Forecasting (ECMWF) models and the identification of the radiometric transformation coefficients derived from the scatter plot of the beacon-derived sky brightness temperature estimates and the noise power measurements, fully described in [2, 4].

Validation of Noise Power Measurement with Radiometer Measurements

In order to validate that the extracted attenuation levels from the integrated noise power measurements produce accurate results, a comparison of the transform procedure utilized for clear sky calibration in this experiment and the direct radiometric measurements made by the PR-2230 was performed. The PR-2230, however, is limited to a minimum 10 deg elevation angle observation due to the wide (~3 deg) beamwidth of the radiometer antenna, therefore, the two systems are not necessarily looking at the same portion of the sky. However, in the scatter plot of Figure 5, it is shown that there is a high degree of correlation with the instantaneous measurements of sky brightness temperature between both the radiometer and integrated noise power measurements. Figure 5 shows example monthly scatterplot data for February 2017 indicating this strong correlation between measurements. Also in Figure 5, is the time series for the month indicating that the absolute levels derived from both the integrated noise power calibration approach and the radiometer approach are in good agreement. The spread in the results are expected due to measurements of non-identical sky and different beamwidths. Less spread in the scatterplot at lower brightness temperature measurements are commensurate with clear sky observations, which would minimize the variation in observations due to different portions of the sky, with wider variations occurring where influence from cloud cover differences at the different observation angles become more pronounced.

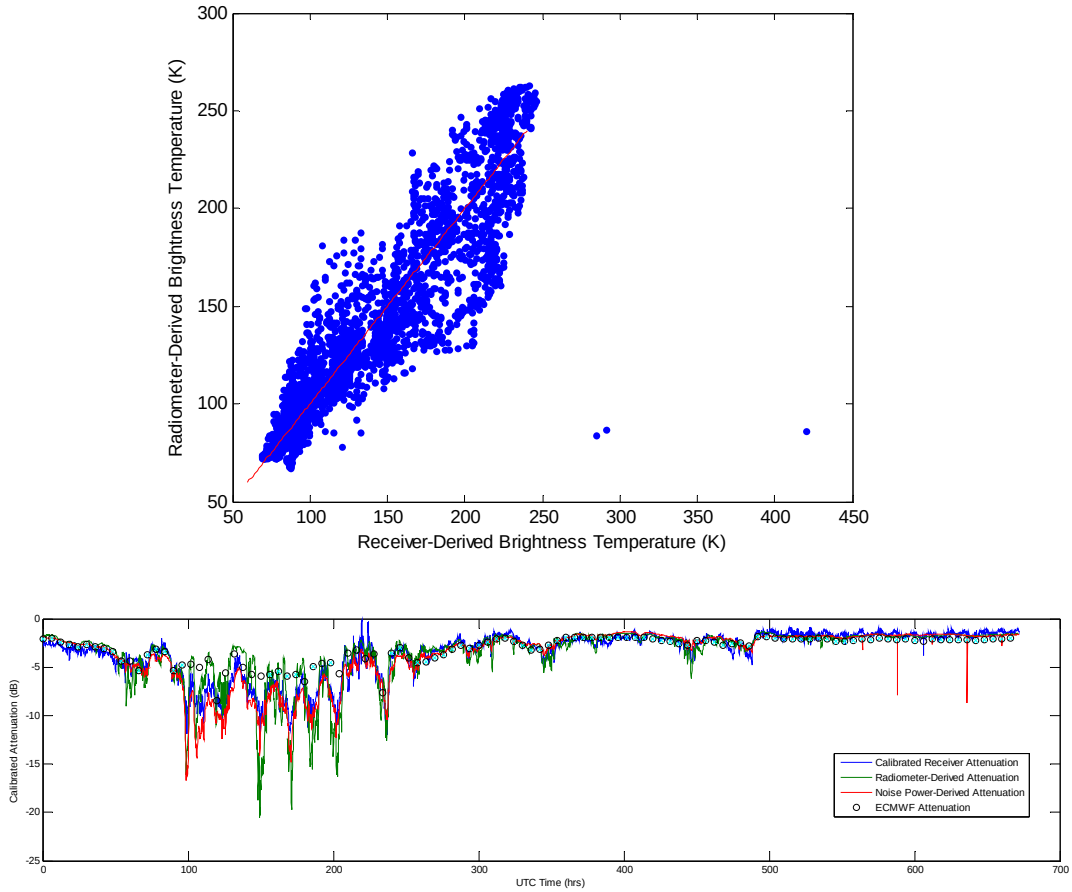

Figure 5. (top) Scatterplot of radiometer-derived brightness temperature at 10 deg elevation angle and noise-power derived brightness temperature (scaled from 2.6 deg to 10 deg) for the month of February 2017. (bottom) Time series comparison of receiver attenuation, radiometer-derived attenuation, noise power-derived attenuation, and ECMWF data for February 2017.

First Year Results

Summary statistics of surface meteorological measurements are presented in Figures 6-7. Figure 6 provides monthly and average annual surface pressure, temperature, relative humidity, and derived water vapor density. Figure 7 provides a comparison of the optical rain gauge and tipping bucket rain rate measurements compared with the ITU model P.837-7. From the experiment campaign, it was observed that the optical rain gauge had difficulty determining rain rate during snow events, resulting in much larger derived rain rates. When this data was removed by eliminating measurements when the surface temperature was below 0 deg C, the resulting rain rate curve is in closer agreement to the tipping bucket and ITU model.

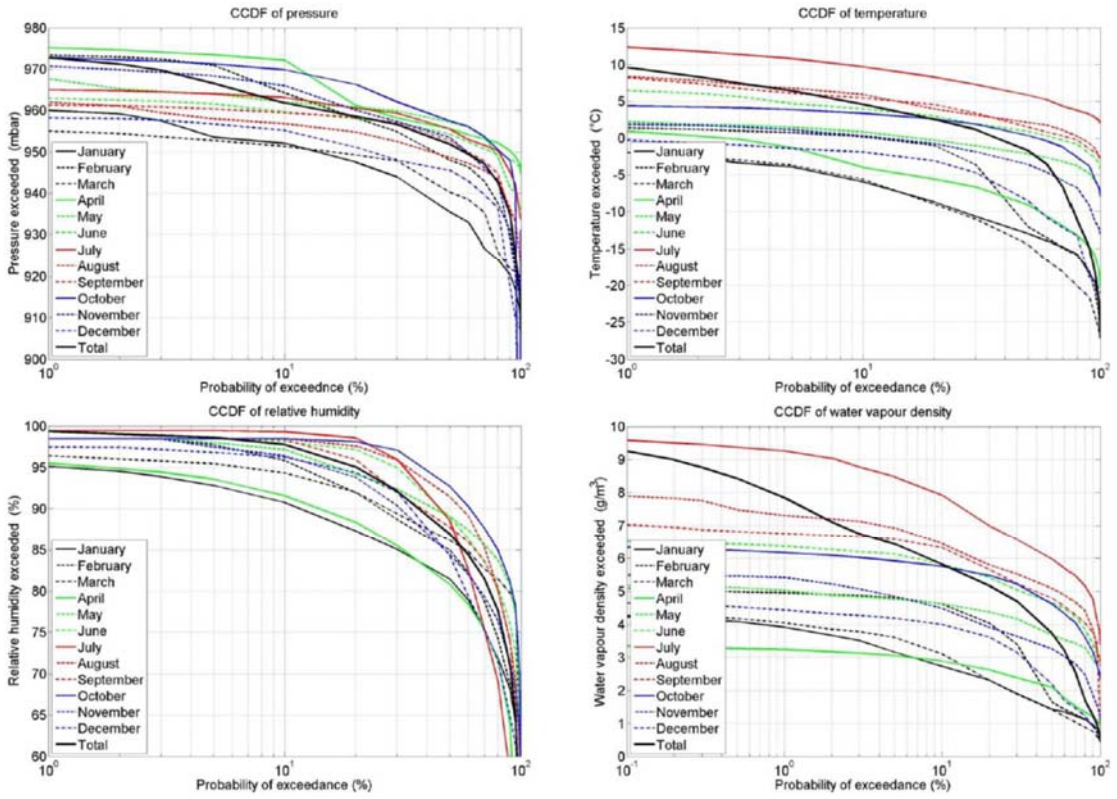

Figure 6. Monthly and average annual CCDFs for temperature, pressure, relative humidity, and derived water vapor density at SG61.

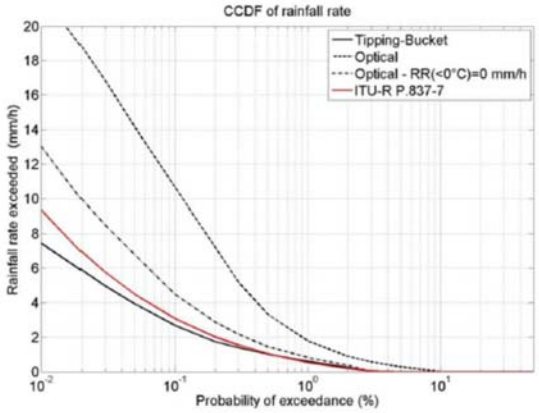

Figure 7. CCDF of rainfall rate comparing tipping bucket and optical rain gauge results with the ITU-R P.837-7 model.

Atmospheric Scintillation

At the extremely low elevation angle of observation from Svalsat, atmospheric scintillation and multipath effects play a large role, resulting in long time scale and deep fading events. This made processing of the data more difficult due to the inherent difficulty of separating out scintillation-induced fades from the standard definition of excess attenuation. Figure 8 below shows two example time series, one in the winter with relatively low scintillation, and one in the summer where the scintillation and/or multipath is shown to approach >10 dB fluctuations. The CCDF for scintillation fade, enhancement, and standard deviation are shown in Figure 9 for one year of measurements.

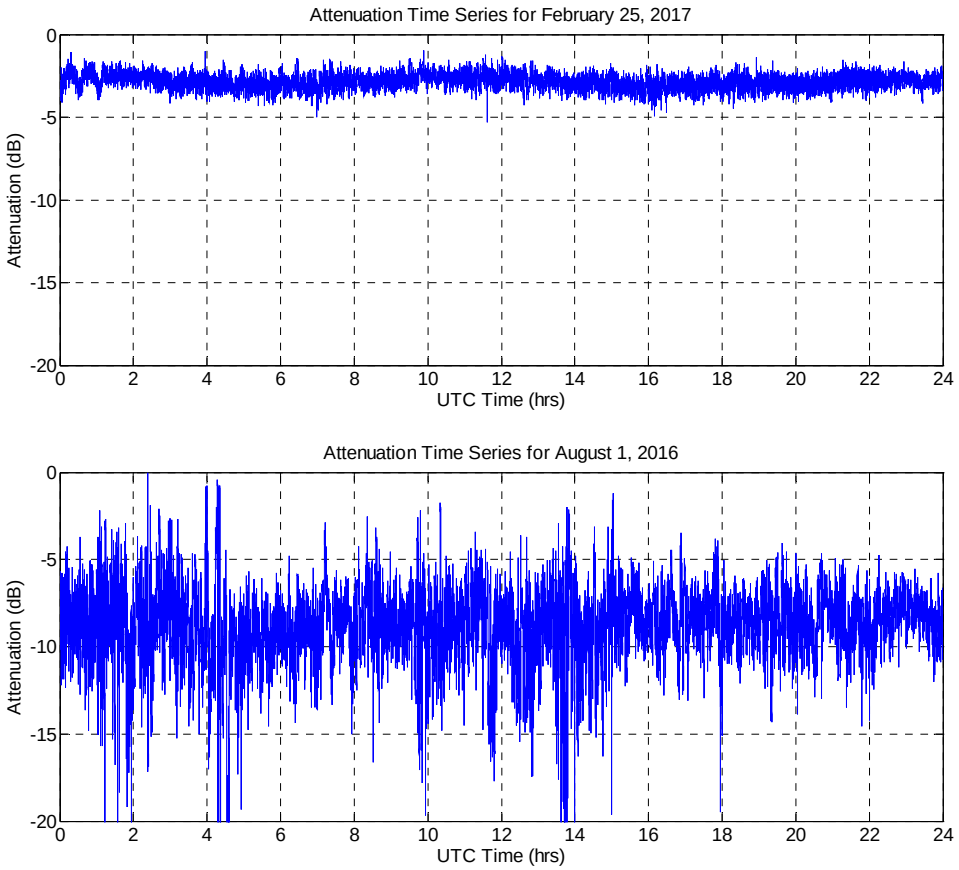

Figure 8. Time series for a winter day (top) and a summer day (bottom) showing the variation and extremes of scintillation fluctuations at the polar site.

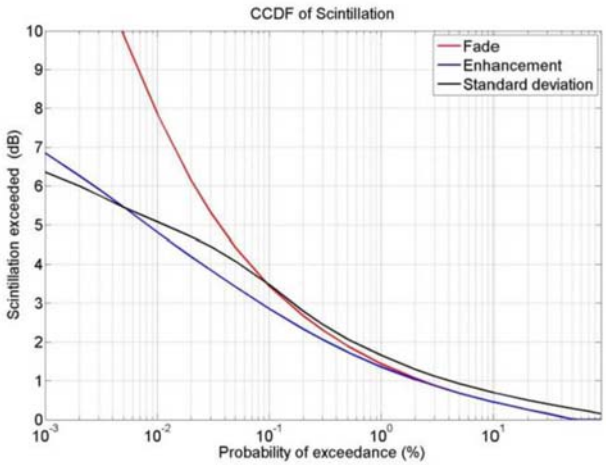

Figure 9. CCDF of scintillation for one year of data.

Total Attenuation

The total attenuation CCDF curves for the first year of measurements are shown plotted below in Figure 10. A plot of the beacon measured attenuation and the radiometer measured attenuation for the year are provided and compared to the ITU-R P.618-12 model. The relatively close agreement between each of these different techniques provides added confidence since the results are consistent with each other.

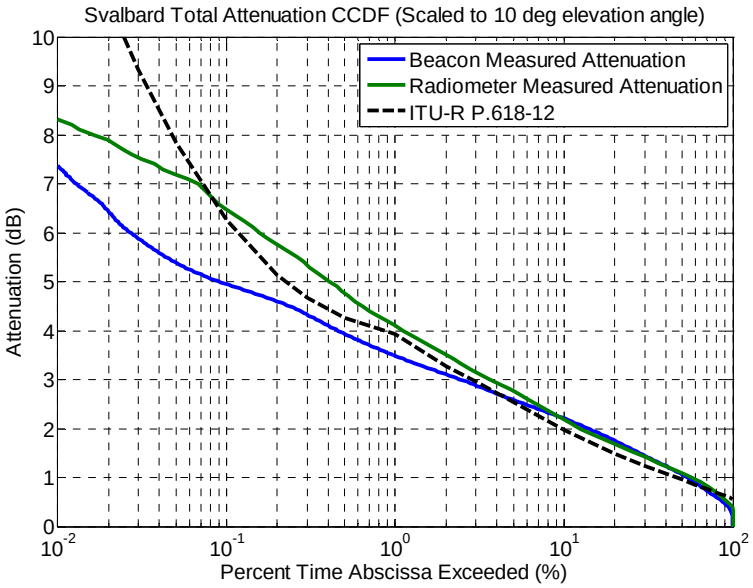

Figure 10. CCDF curves for beacon, radiometer, and model-predicted attenuation at Svalbard for one year.

At 99% availability, which is the assumed target for NASA polar orbiting missions, the measurements from the radiometric and beacon observations agree within 1 dB of each other and the model. However, it should be noted that these curves are based on available data for the common year that both were in operations, but are not concurrent. Furthermore, the beacon measurements are scaled to 10 deg from a 2 deg observation elevation angle, and may introduce some errors resulting in this deviation.

Conclusions

One year of statistical results from beacon measurements are presented for the site characterization campaign in Svalbard. Between model, beacon, and radiometer measurements, consistent statistical results were obtained, particularly during the non-scattering availabilities (<98% availability), giving confidence to the results. Data collection has continued for an additional year, and further refinement of the statistics and processing results will be performed to continue to enhance the characterization of the polar atmosphere for future earth observation missions employing Ka-band direct to earth links.

References

[1] J. Nessel, M. Zemba, J. Morse, "Results from Three Years of Ka-band Propagation Characterization at Svalbard, Norway," 9th European Conference on Antennas and Propagation, April 2015.

[2] J. Nessel, J. Morse, M. Zemba, C. Riva, L. Luini, "Preliminary Results of the NASA Beacon Receiver for Alphasat Aldo Paraboni TDP5 Propagation Experiment," 20th Ka and Broadband Communications Conference, Salerno, Italy, October 2014.

[3] J. Nessel, G. Goussetis, M. Zemba, J. Houts, A. Costouri, "Design and Preliminary Results from Edinburgh, UK, Alphasat Q-band Propagation Terminal," 22nd Ka and Broadband Communications Conference, Cleveland, OH, October 2016.

[4] L. Luini, C. Riva, C. Capsoni, A. Martellucci, "Attenuation in Nonrainy Conditions at Millimeter Wavelengths: Assessment of a Procedure," IEEE Trans. On Geo. And Rem. Sens., Vol. 45, No. 7, July 2007.